

Moiré superlattices arising from growth induced by screw dislocations in layered materials

Fuyu Tian(田伏钰), Muhammad Faizan, Xin He(贺欣), Yuanhui Sun(孙远慧), and Lijun Zhang(张立军)
Citation: Chin. Phys. B, 2024, 33 (**7**): 077403. DOI: 10.1088/1674-1056/ad4cdc
Journal homepage: http://cpb.iphy.ac.cn; http://iopscience.iop.org/cpb

What follows is a list of articles you may be interested in

Enhanced ferromagnetism and conductivity of ultrathin freestanding $La_{0.7}Sr_{0.3}MnO_3$ membranes

Siqi Shan(单思齐), Yequan Chen(陈业全), Yongda Chen(陈勇达), Wenzhuo Zhuang(庄文卓), Ruxin Liu(刘汝新), Xu Zhang(张旭), Rong Zhang(张荣), and Xuefeng Wang(王学锋)
Chin. Phys. B, 2023, 32 (**10**): 107402. DOI: 10.1088/1674-1056/ace161

Customizing topological phases in the twisted bilayer superconductors with even-parity pairings

Conghao Lin(林丛豪), Chuanshuai Huang(黄传帅), and Xiancong Lu(卢仙聪)
Chin. Phys. B, 2023, 32 (**8**): 087401. DOI: 10.1088/1674-1056/acd3e3

Superconducting anisotropy and vortex pinning in $CaKFe_4As_4$ and $KCa_2Fe_4As_4F_2$

A B Yu(于奥博), Z Huang(黄喆), C Zhang(张驰), Y F Wu(吴宇峰), T Wang(王腾), T Xie(谢涛), C Liu(刘畅), H Li(李浩), W Peng(彭炜), H Q Luo(罗会仟), G Mu(牟刚), H Xiao(肖宏), L X You(尤立星), and T Hu(胡涛)
Chin. Phys. B, 2021, 30 (**2**): 027401. DOI: 10.1088/1674-1056/abcf98

Phase-field simulation of superconductor vortex clustering in the vicinity of ferromagnetic domain bifurcations

Hasnain Mehdi Jafri, Jing Wang(王静), Chao Yang(杨超), Jun-Sheng Wang(王俊升), and Hou-Bing Huang(黄厚兵)
Chin. Phys. B, 2020, 29 (**12**): 127402. DOI: 10.1088/1674-1056/abb22c

Evidence for topological superconductivity: Topological edge states in Bi_2Te_3/FeTe heterostructure

Bin Guo(郭斌), Kai-Ge Shi(师凯歌), Hai-Lang Qin(秦海浪), Liang Zhou(周良), Wei-Qiang Chen(陈伟强), Fei Ye(叶飞), Jia-Wei Mei(梅佳伟), Hong-Tao He(何洪涛), Tian-Luo Pan(潘天洛), Gan Wang(王干)
Chin. Phys. B, 2020, 29 (**9**): 097403. DOI: 10.1088/1674-1056/abaf9c

---

RAPID COMMUNICATION

Moiré superlattices arising from growth induced by screw dislocations in layered materials

Fuyu Tian(田伏钰)[1], Muhammad Faizan[1], Xin He(贺欣)[1], Yuanhui Sun(孙远慧)[2,†], and Lijun Zhang(张立军)[1,‡]

[1] *State Key Laboratory of Integrated Optoelectronics Key Laboratory of Automobile Materials of MOE and College of Materials Science and Engineering, Jilin University, Changchun* 130012, *China*

[2] *Suzhou Laboratory, Suzhou* 215123, *China*

(Received 26 April 2024; revised manuscript received 16 May 2024; accepted manuscript online 17 May 2024)

Moiré superlattices (MSLs) are modulated structures produced from homogeneous or heterogeneous two-dimensional layers stacked with a twist angle and/or lattice mismatch. Enriching the methods for fabricating MSL and realizing the unique emergent properties are key challenges in its investigation. Here we recommend that the spiral dislocation driven growth is another optional method for the preparation of high quality MSL samples. The spiral structure stabilizes the constant out-of-plane lattice distance, causing the variations in electronic and optical properties. Taking SnS_2 MSL as an example, we find prominent properties including large band gap reduction (~ 0.4 eV) and enhanced optical activity. First-principles calculations reveal that these unusual properties can be ascribed to the locally enhanced interlayer interaction associated with the Moiré potential modulation. We believe that the spiral dislocation driven growth would be a powerful method to expand the MSL family and broaden their scope of application.

Keywords: Moiré superlattices, interlayer interaction, spiral dislocation, layered materials

PACS: 74.78.Fk, 68.65.Cd, 31.15.es, 81.10.–h **DOI:** 10.1088/1674-1056/ad4cdc

1. Introduction

Two-dimensional (2D) layered materials have attracted considerable interest in recent years owing to their potential applications in nanomaterials and optoelectronics.[1–6] In addition to a variety of materials and the dependence of layer thickness, stacking 2D layers into artificial van der Waals heterostructures also provides degrees of freedom to engineer their electronic and optical properties.[7,8] The resulting modulated strain field and electrostatic potential combined with the ubiquitous interlayer coupling may give rise to distinct emergent physical properties,[23–26] for example, the Hofstadter butterfly spectra,[17,27–29] cloned Dirac Fermions,[17–19] fractional quantum Hall effects[28–30] and topological mosaics[31] in graphene-based and transition metal dichalcogenides-based Moiré superlattices (MSLs). Thus far, researchers have realized the MSLs fabrication by wet transfer of mechanically exfoliated monolayers,[32–35] epitaxial growth,[36–38] one-pot solvothermal approaches,[39] and so forth. The commonly used method to fabricate MSLs through stacking together mechanically exfoliated monolayers suffers from issues of uncontrolled stacking patterns and registry, contamination at the interfaces, and sample uniformity/size limitations.[32–35] Recently, epitaxial growth approach (e.g., chemical vapor deposition) can in principle overcome these problems, but are not yet widely reported.[36–38] Here, we suggest that the spiral dislocation driven growth is another desirable method for the preparation of high quality MSLs samples.

In addition to layer-by-layer growth, a series of 2D spiral structures have been recently driven by screw dislocations under low supersaturation condition (Fig. 1(a)).[39–49] Careful structural and spectroscopic analysis revealed that these spiral structures possess a variety of stacking patterns, such as triangular, tetragonal, hexagonal, and triangular–hexagonal mixed shapes. A schematic representation of the incorporation of screw dislocation from layer-by-layer structure to spiral structure is shown in Fig. 1(b). Through the investigation of these cases, except for SnSe and Bi_2Se_3, almost all in-plane x-ray diffraction (XRD) peaks of these compounds are missing. Based on high-resolution transmission electron microscope and second-harmonic generation measurements, Fan *et al.* identified that a twist angle of 5° is formed between the top and bottom layers in spiral WS_2.[42] Additionally, the selected area diffraction measurement clearly shows two sets of diffraction spots with angles ranging from 1.6° to 3° occurred in spiral BiOCl.[39] Thus we speculate that the peaks missing in XRD spectra should be attributed to the appearance of small twist angle in the spiral plates. As illustrated in the left panel of Fig. 1(c), the same diffraction angle in the layer-by-layer growth structure will cause the superimposition of diffraction intensity for a given lattice plane. On the contrary, the appearance of twist angle (θ) between two adjacent spiral layers breaks the in-plane lattice periodicity, losing the ability to

†Corresponding author. E-mail: sunyh@szlab.ac.cn

‡Corresponding author. E-mail: lijun_zhang@jlu.edu.cn

© 2024 Chinese Physical Society and IOP Publishing Ltd

superimpose the in-plane diffraction intensity (right panel of Fig. 1(c)). However, its periodicity along out-of-plane direction is maintained with the growth of spiral plates, causing the relative diffraction intensity of in-plane peaks to visually decrease to a negligible level. Hence we believe that MSLs can be obtained through screw dislocation driven growth with a processing method to form a small twist angle. An easy way to confirm its formation is by checking the disappearance of in-plane peaks in the XRD spectra of synthesized spiral plates. To be more precise, one can intuitively observe the explicit atomic arrangements of selected regions by performing scanning transmission electron microscope analysis.[38,39]

(a)

Spiral plates	In-plane peaks
SnSe	Retention
Bi_2Se_3	Retention
MoS_2	Missing
WSe_2	Missing
HfS_2	Missing
SnS_2	Missing

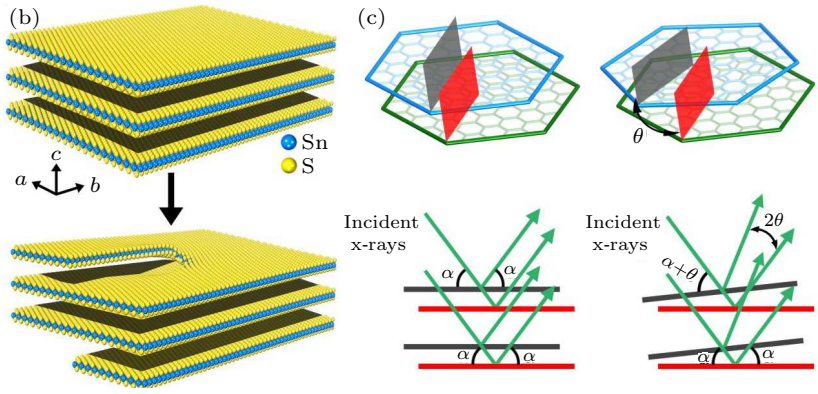


Fig. 1. Explanation of the formation of MSLs in the spiral plates with a small twist angle. (a) A series of 2D spiral plates recently driven by screw dislocations under low supersaturation condition. In addition, the retention or missing of in-plane peaks is also shown. (b) Schematic representation of the incorporation of screw dislocation from layer-by-layer structure to spiral structure. (c) Schematic representation of XRD of 2D plates without or with a small twist angle.

In this work, we take SnS_2 MSL as an example to investigate its electronic and optical properties. Xia *et al.* successfully synthesized a large scale of 2D spiral SnS_2 crystals by using a simple atmospheric pressure vapor deposition method.[46] The good photo-stability and reproducibility as well as a fast photoresponse time enable the SnS_2 to be a promising candidate for photodetectors. The in-plane peaks missing in its XRD spectrum indicate the existence of a small twist angle. On the other hand, the diffraction reflections indexed to $(000N)$ $(N = 0, 1, 2, \ldots)$ planes have the same diffraction angles as bulk SnS_2, which denotes that the spiral SnS_2 crystals grow preferably along out-of-plane direction with the same interlayer distance as bulk SnS_2. Hence we conclude that the SnS_2 MSL with a constant interlayer distance has been synthesized. However, the large wavelength of the Moiré potential results in great MSL complexity, posing challenges for both theoretical and experimental investigations of its properties. Theoretically speaking, it is very challenging to use a large unit cell for electronic structure calculations with density functional theory (DFT). In addition to the most commonly used tight binding-based method,[50–54] large-scale DFT simulations based on linear combination of atomic orbitals or linearly scaling 3D fragment methods have also been used for the investigation of MSLs.[55–58] However, the MSL period reaches the order of tens of nanometers under a small lattice mismatch or small twist angle,[14,38,39,50,55,59–61] which is dozens of times that of common crystals. In addition to the fascinating properties of MSLs as a whole, the property variations at different local positions within the MSLs are also important for the understanding of material characteristics. In this work, we recommend another method to simulate the property variations throughout the MSL, which has consistently described the experimental observation of spiral BiOCl.[39] We note that our method is only suitable for the investigation of MSL with a small twist angle.

2. Computational methods

First-principles calculations were carried out within the framework of density functional theory by using plane-wave pseudopotential methods as implemented in the Vienna *Ab-initio* Simulation Package.[62,63] The electron–ion interactions were described by using the projected augmented wave pseudopotentials with the $5s^25p^2$ (Sn) and $3s^23p^4$ (S) treated explicitly as valence electrons. We used the generalized gradient approximation formulated by Perdew, Burke, and Ernzerhof[64] as the exchange–correlation functional. The layered SnS_2 structures were embedded in a vacuum region with 30 Å thickness. A kinetic energy cutoff of 520 eV was used for wave-function expansion, and a $31 \times 31 \times 1$ k-point grid within the Monkhorst–Pack scheme was adopted for electronic Brillouin zone integration. The optB86b-vdW functional[65] was used to describe the dispersive van der Waals interaction, which was found to give a good agreement with experimental lattice parameters.[66] The cell parameters and internal atomic positions were obtained using the conjugate gradient technique until the total energies converged to less than 10^{-5} eV. The interlayer distance of the constructed SnS_2 structures was fixed at 0.592 Å (the same interlayer distance as bulk SnS_2)[66] during the structure optimization.

3. Results and discussion

To give an intuitive impression of SnS_2 MSL, a topological SnS_2 bilayer structure with 3.1° twist angle is constructed as shown in the perpendicular view in Fig. 2(a). When two adjacent spiral layers form a small twist angle θ, the period L of such MSL is given by $L = a_0/\sin\theta \approx a_0/\theta$, where a_0 is the length of in-plane Bravais lattice (0.365 Å for SnS_2).[66] This leads to the formation of a periodic MSL structure with a period 6.75 nm, containing 662 SnS_2 units (1986 atoms). The periodic length will significantly increase if a smaller twist angle is formed in the spiral structure. For example, the periodicity is 20.91 nm when $\theta = 1.0°$, which contains more than 1.9×10^4 atoms in SnS_2 MSL. To avoid the costly calculations, it is necessary to find an easier way to investigate the electronic properties of SnS_2 MSL. Another problem is the non-negligibly internal properties of such a large structure, which deserves an in-depth study to deepen the understanding of MSL structures.

Through the analysis of the structure, we identify that the local interlayer stacking pattern in MSL regularly transfers with the position vector. For example, the local interlayer stacking patterns along four typical paths (path I–IV) reveal that the upper layer moves perpendicularly towards the path direction (Figs. 2(b) and S1). We realize that, by extension, the local interlayer stacking patterns in MSL can be regarded as the regular movement of upper unit with respect to the lower unit. It is worthwhile mentioning that this rule is valid for all MSLs with a small twist angle. Here we adopt a 13×13 point mesh to slice the rhombus SnS_2 MSL, for comparison, we separately computed the structures with fixed and variable interlayer distance (Fig. S2) and found that their bandgap variation trends are consistent, albeit to varying degrees. Based on prior research,[39] the formation of a spiral dislocation structure can effectively stabilize the lattice distance and transfer stress to the center of the spiral dislocation. In order to be consistent with experimental observation, the sliced local structures are set with a constant interlayer distance of 0.592 Å[66] and are fixed during the structure optimization. The small twist angles in all local stacking structures are treated as zero to satisfy the periodic boundary condition. This approximation is based on the expectation that the characteristics of local interlayer interactions are mainly determined by the local stacking patterns and are minimally affected by the small twist angle. According to this method, we have successfully verified the band gap reduction ($\sim$ 0.6 eV) and the increase in carrier lifetime of spiral BiOCl MSL.[39] As shown in Fig. 2(c), we provide the atomic structures at four high symmetry regions, namely, AA, SS, BR, and AB structures, where AA structure is the ground-state stacking pattern of bulk SnS_2, SS structure denotes the head-to-head arrangement of the S atoms from adjacent layers, the Sn-upper atom in BR structure locates on the bridge of two Sn-lower atoms, and the Sn-upper atom in AB structure locates on the top of the S-lower atom.

To explore the evolution of interlayer interactions in SnS_2 MSL, we performed DFT calculations on the electronic properties of local stacking patterns. As shown in Fig. 3(a) and Table S1, the spatially resolved band gap ($E_g(\boldsymbol{r})$) of SnS_2 MSL shows strong dependence on position $\boldsymbol{r}$ (with a counterclockwise rotation of 90° with respect to the MSL in Fig. 2(b)), varying from the minimum 1.11 eV in the area around SS region to the maximum 1.51 eV of AA structure. Our calculations demonstrate a 0.40 eV band gap reduction of SnS_2 upon the emergence of MSL. To confirm the suitability of GGA-PBE exchange–correlation, the HSE06 hybrid functional method was chosen for parallel comparison,[67] which returned a comparable band gap reduction of 0.37 eV. Furthermore, we separately aligned the energies of conduction band minimums (CBMs) and valence band maximums (VBMs) with respect to the corresponding vacuum levels for the 13×13 local stacking patterns of SnS_2 MSL (see Figs. S3(a) and S3(b)), both of them exhibit the triple rotation symmetry similar to the spatially resolved band gap. The global minimums of CBM map and the global maximums of VBM map are both located in the same area around SS structure (see Tables S2 and S3), indicating the in-site transition of SnS_2 MSL in real space. To confirm the accuracy, a large-scale first-principles calculation code[56] is recommended to make the comparison. The calculated charge distributions of CBM and VBM of bilayer SnS_2 MSL with a 3.1° twist angle are shown in Figs. S3(c) and S3(d), which are similar to the spatially resolved band-edge maps from our method. This similarity enhances the credibility of our simulations.

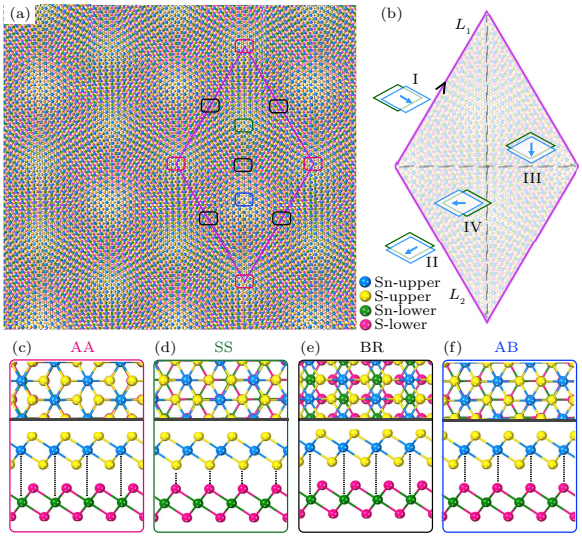


Fig. 2. Atomic structures of SnS_2 spiral bilayer MSL. (a) Perpendicular view of the topological SnS_2 spiral bilayer structure with a twist angle of 3.1°, forming a MSL with the periodicity $L = 6.75$ nm. (b) Four typical paths of the SnS_2 MSL shown in the pink rhombus in (a). (c)–(f) Top and side views of the bilayer structures at four high symmetry regions marked in (a), namely, AA, SS, BR, and AB structures, which are indicated by red, green, black, and blue squares, respectively.

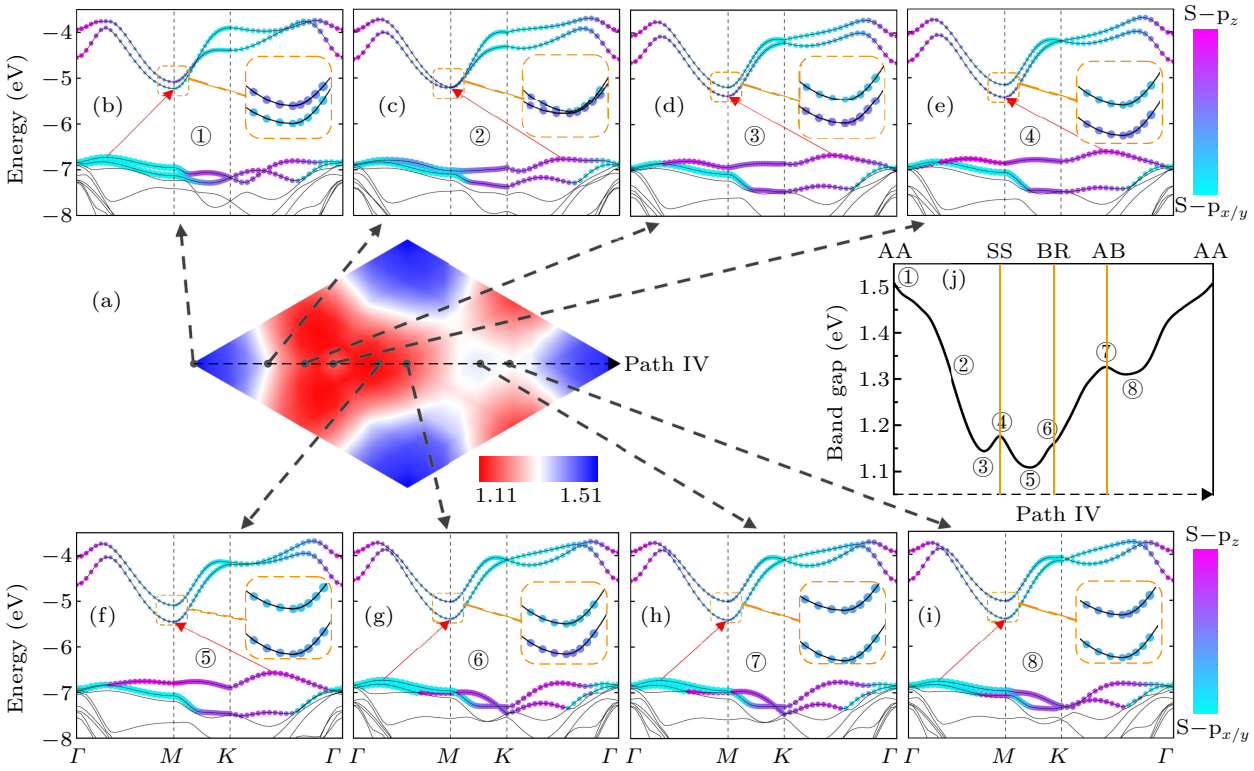


Fig. 3. Electronic properties of SnS_2 spiral bilayer MSL. (a) Spatially resolved band gaps of SnS_2 MSL. (b)–(i) Calculated band structures of crucial stacking patterns along path IV. The band structures have been projected onto atomic orbitals with the weight of the out-of-plane S-p_z and the in-plane S-$p_{x/y}$ orbitals. (j) Evolution of band gaps for the local stacking structures along path IV.

Because the four high-symmetry stacking patterns and the regions of band gap minimum/maximum are all located on path IV, we will take it as an example to explain the band gap reduction in SnS_2 MSL. Figures 3(b)–3(i) illustrate the evolution of band structures of the local stacking patterns along path IV, and the corresponding evolution of band gaps is plotted in Fig. 3(j). For the convenience of comparison, their orbital energies are all aligned to the vacuum levels. We can see that the band structures of eight chosen stacking patterns all hold the indirect band gap transition character. Moreover, both CBM and VBM contribute to the band gap reduction in SnS_2 MSL according to their evolutions as shown in Fig. S4. As the position vector moves along path IV, CBM always locates at M point, while the location of VBM first transfers from Γ–M path to Γ–K path accompanying with the band gap decrease to the global minimum, then it transfers back to Γ–M path with an increase in the band gap. To further understand this, the in-plane $p_{x/y}$ orbital and the out-of-plane p_z orbital of S atoms are projected separately for the four bands near the Fermi level. The close-up image in Fig. 3(b) shows that CBM and the second CBM of AA structure are mainly contributed by the in-plane $p_{x/y}$ orbital and the out-of-plane p_z orbital of S atoms, respectively. As the band gap decreases, the p_z orbital descends faster than the $p_{x/y}$ orbital and surpasses the latter to become the new CBM at position ②. Their energy difference reaches the maximum at position ⑤, which is also the stacking region where the band gap is the global minimum. Then the p_z orbital gradually ascends and once again becomes the second CBM with the band gap increasing. To some extent, the situation of VBM is similar to that of CBM. It is mainly occupied by the in-plane $p_{x/y}$ orbital concentrated at Γ–M path in AA structure, then at position ② the out-of-plane p_z orbital concentrated at Γ–K path takes over the contribution to VBM until position ⑤. Soon afterwards, the VBM is occupied by the $p_{x/y}$ orbital concentrated at Γ–M path and continues to the end. We conclude that both the downward shifting CBM and the upward shifting VBM in the area around SS structure are dominated by the p_z orbital, which arises from the short distance of head-to-head arrangement of S atoms from adjacent layers. Furthermore, the relevant charge distributions of CBM and VBM for eight stacking structures along path IV are shown in Fig. S5, we can clearly see that the charges of VBM at position ③–⑤ are distributed along the out-of-plane direction. The locally enhanced interlayer interaction upon appearance of MSL is responsible for the large band gap reduction in SnS_2 MSL.

To probe the potential effects of distinct regions under different stacking patterns on optical activities of SnS_2 MSL, we calculated the wave function overlap between VBM and CBM, $\int |\psi^*_{\mathrm{VBM}}||\psi_{\mathrm{CBM}}|\,\mathrm{d}r^3$, which is closely relevant to the intensity of optical transition, carrier lifetime exciton binding, and so forth. The spatially resolved overlap integrals of SnS_2 MSL are shown in Fig. 4(a), in which the value of AA structure is normalized for comparison. We can see that most

regions in SnS_2 MSL manifest the enhanced optical activity with respect to AA structure, especially for the stacking regions along AA → SS path (Table S4). Furthermore, we have also investigated the wave function overlap behavior for direct band gap transition (Fig. 4(b) and Table S5). It shows the enhanced overlap capability with respect to AA region, however, the mostly enhanced regions are around SS and AB structures. Strikingly, the distribution map of overlap integrals for direct band gap transition is consistent with that of spatially resolved band gap in real-space, which indicates the usability in optoelectronics.

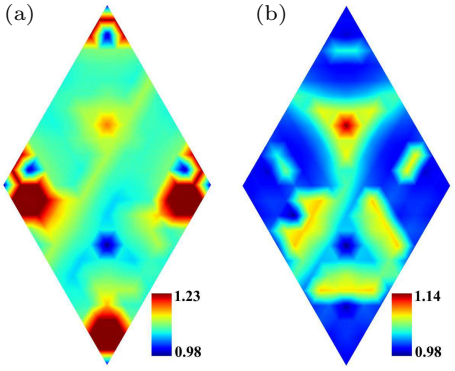


Fig. 4. Optical activity of SnS_2 spiral bilayer MSL. Spatially resolved overlap integrals of (a) indirect band gap transition and (b) direct band gap transition of SnS_2 MSL. The value of AA structure is normalized for comparison.

4. Conclusion

In conclusion, we propose that the MSL can be obtained through screw dislocation driven growth with a processing method to form a small twist angle, which provides more potential for the field of MSL materials. Taking SnS_2 MSL as an example, we investigate its position-dependent electronic and optical properties. First-principles calculations show that the spatially resolved band gap exhibits a considerable reduction of 0.4 eV with respect to bilayer SnS_2. According to the detailed analysis along the high symmetry path IV in the SnS_2 MSL, we demonstrate that the considerable decrease/increase of CBM/VBM at regions around SS structure is dominated by the out-of-plane p_z orbital, associating with locally enhanced interlayer interaction. On the other hand, the significantly enhanced optical activity of indirect/direct band gap transition in SnS_2 MSL is verified by using the wave function overlap integrals method. Although our method cannot perfectly describe the structural characteristics, it is still qualitatively sufficient to guide the exploration of 2D MSLs.

The screw dislocation-driven MSL approach is expected to be expanded in transition metal dichalcogenides (TMDs) and other materials. Currently, spiral structures are experimentally synthesized mainly based on vapor deposition methods. For example, large-size 2D SnS_2 crystals were prepared on mica sheets by screw-dislocation-driven (SDD), its possible mechanisms of generation and expansion were explained. The prepared photodetectors exhibited excellent photostability, reproducibility and optical response time.[46] Meanwhile, Madoune *et al.* investigated the growth mechanism of spiral pyramidal WS_2 formed based on physical vapor deposition and its interesting optical properties using atomic force microscopy and Raman spectroscopy.[47] The first large-scale synthesis of spiral $MoSe_2$ via flux-controlled chemical vapor deposition method was reported by Ahn *et al.*, resulting in significant enhancement of the nonlinear optical signals attributed to the combination of broken inversion symmetry and exciton resonance effects.[48] These studies highlight the feasibility of employing spiral dislocation-driven methods to modulate MSL configurations in TMD materials. Nevertheless, deeper theoretical investigations are warranted to comprehend underlying structural mechanisms. Instructively, Ouyang *et al.* reviewed the structural evolution of spiral nanopyramids, spiral nanowires, etc., emphasizing the enhanced light–matter interactions and device physics.[49] While MSL represents a promising method for modulating TMDs, theoretical research in this area remains limited. Our proposed theoretical mechanisms for small-angle twisted MSL formed by spiral dislocations enrich theoretical frameworks, presenting new opportunities for optoelectronic devices and customized designs. Spiral dislocation-driven growth methods will be a potent means to expand the MSL family and diversify its applications.

Acknowledgments

Project supported by the National Key Research and Development Program of China (Grant No. 2022YFA1402500) and the National Natural Science Foundation of China (Grant No. 62125402). Calculations were performed in part at the high performance computing center of Jilin University.

References

[1] Mak K F, Lee C, Hone J, Shan J and Heinz T F 2010 *Phys. Rev. Lett.* **105** 136805
[2] Yin X, Ye Z, Chenet D A, Ye Y, O'Brien K, Hone J C and Zhang X 2014 *Science* **344** 488
[3] Wu S, Buckley S, Schaibley J R, Feng L, Yan J, Mandrus D G, Hatami F, Yao W, Vučković J, Majumdar A and Xu X X 2015 *Nature* **520** 69
[4] Yang T, Zheng B, Wang Z, Xu T, Pan C, Zou J, Zhang X, Qi Z, Liu H, Feng Y, Hu W, Miao F, Sun L, Duan X and Pan A 2017 *Nat. Commun.* **8** 1906
[5] Xu M, Liang T, Shi M and Chen H 2013 *Chem. Rev.* **113** 3766
[6] Huang Y, Sutter E, Sadowski J T, Cotlet M, Monti O L A, Racke D A, Neupane M R, Wickramaratne D, Lake R K, Parkinson B A and Sutter P 2014 *ACS Nano* **8** 10743
[7] Geim A K and Grigorieva I V 2013 *Nature* **499** 419
[8] Novoselov K S, Mishchenko A, Carvalho A and Neto A H C 2016 *Science* **353** aac9439
[9] Miller D L, Kubista K D, Rutter G M, Ruan M, de Heer W A, First P N and Stroscio J A 2009 *Science* **324** 924
[10] Luican A, Li G, Reina A, Kong J, Nair R R, Novoselov K S, Geim A K and Andrei E Y 2011 *Phys. Rev. Lett.* **106** 126802
[11] Li G, Luican A, Lopes dos Santos J M B, Castro Neto A H, Reina A, Kong J and Andrei E Y 2010 *Nat. Phys.* **6** 109
[12] MacDonald A H and Bistritzer R 2011 *Nature* **474** 453

[13] Yu G L, Gorbachev R V, Tu J S, Kretinin A V, Cao Y, Jalil R, Withers F, Ponomarenko L A, Piot B A, Potemski M, Elias D C, Chen X, Watanabe K, Taniguchi T, Grigorieva I V, Novoselov K S, Fal'ko V I, Geim A K and Mishchenko A 2014 *Nat. Phys.* **10** 525

[14] Brihuega I, Mallet P, González-Herrero H, Trambly de Laissardière G, Ugeda M M, Magaud L, Gómez-Rodríuez J M, Ynduráin F and Veuillen J Y 2012 *Phys. Rev. Lett.* **109** 196802

[15] Yao W, Wang E, Bao C, Zhang Y, Zhang K, Bao K, Chan C K, Chen C, Avila J, Asensio M C, Zhu J and Zhou S 2018 *Proc. Natl. Acad. Sci. USA* **115** 6928

[16] Cao Y, Fatemi V, Fang S, Watanabe K, Taniguchi T, Kaxiras E and Jarillo-Herrero P 2018 *Nature* **556** 43

[17] Yankowitz M, Xue J, Cormode D, Sanchez-Yamagishi J D, Watanabe K, Taniguchi T, Jacquod P, Jarillo-Herrero P and LeRoy B J 2012 *Nat. Phys.* **8** 382

[18] Ci L, Song L, Jin C, Jariwala D, Wu D, Li Y, Srivastava A, Wang Z F, Storr K, Balicas L, Liu F and Ajayan P M 2010 *Nat. Mater.* **9** 430

[19] Chen Z G, Shi Z, Yang W, Lu X, Lai Y, Yan H, Wang F, Zhang G and Li Z 2014 *Nat. Commun.* **5** 4461

[20] Ahn S J, Moon P, Kim T H, Kim H W, Shin H C, Kim E H, Cha H W, Kahng S J, Kim P, Koshino M, Son Y W, Yang C W and Ahn J R 2018 *Science* **361** 782

[21] Yankowitz M, Jung J, Laksono E, Leconte N, Chittari B L, Watanabe K, Taniguchi T, Adam S, Graf D and Dean C R 2018 *Nature* **557** 404

[22] Cao Y, Fatemi V, Demir A, Fang S, Tomarken S L, Luo J Y, Sanchez-Yamagishi J D, Watanabe K, Taniguchi T, Kaxiras E, Ashoori R C and Jarillo-Herrero P 2018 *Nature* **556** 80

[23] Jat M K, Tiwari P, Bajaj R, Shitut I, Mandal S, Watanabe K, Taniguchi T, Krishnamurthy H R, Jain M and Bid A 2024 *Nat. Commun.* **15** 2335

[24] Zheng H H, Guo H L, Chen S L, Wu B, Li S F, He J, Liu Z W, Lu G, Duan X D, Pan A and Liu Y P 2023 *Adv. Mater.* **35** 2210909

[25] Liu Y P, Zeng C, Yu J, Zhong J H, Li B, Zhang Z W, Liu Z W, Wang Z M, Pan A and Duan X D 2021 *Chem. Soc. Rev.* **50** 6401

[26] Zheng H H, Wu B, Li S F, Ding J N, He J, Liu Z W, Wang C T, Wang J T, Pan A and Liu Y P 2023 *Light-Sci. Appl.* **12** 117

[27] Ponomarenko L, Gorbachev R, Yu G, Elias D, Jalil R, Patel A, Mishchenko A, Mayorov A, Woods C and Wallbank J 2013 *Nature* **497** 594

[28] Yang W, Lu X, Chen G, Wu S, Xie G, Cheng M, Wang D, Yang R, Shi D, Watanabe K, Taniguchi T, Voisin C, Plaçais B, Zhang Y and Zhang G 2016 *Nano Lett.* **16** 2387

[29] Dean C R, Wang L, Maher P, Forsythe C, Ghahari F, Gao Y, Katoch J, Ishigami M, Moon P, Koshino M, Taniguchi T, Watanabe K, Shepard K L, Hone J and Kim P 2012 *Nature* **497** 598

[30] Fang H, Battaglia C, Carraro C, Nemsak S, Ozdol B, Kang J S, Bechtel H A, Desai S B, Kronast F, Unal A A, Conti G, Conlon C, Palsson G K, Martin M C, Minor A M, Fadley C S, Yablonovitch E, Maboudian R and Javey A 2014 *Proc. Natl. Acad. Sci. USA* **111** 6198

[31] Tong Q, Yu H, Zhu Q, Wang Y, Xu X and Yao W 2016 *Nat. Phys.* **13** 356

[32] Yankowitz M, Xue J, Cormode D, Sanchez-Yamagishi J D, Watanabe K, Taniguchi T, Jarillo-Herrero P, Jacquod P and LeRoy B J 2012 *Nat. Phys.* **8** 382

[33] Dean C R, Young A F, Cadden-Zimansky P, Wang L, Ren H, Watanabe K, Taniguchi T, Kim P, Hone J and Shepard K L 2011 *Nat. Phys.* **7** 693

[34] Xue J, Sanchez-Yamagishi J, Bulmash D, Jacquod P, Deshpande A, Watanabe K, Taniguchi T, Jarillo-Herrero P and LeRoy B J 2011 *Nat. Mater.* **10** 282

[35] Dean C R, Young A F, Meric I, Lee C, Wang L, Sorgenfrei S, Watanabe K, Taniguchi T, Kim P, Shepard K L and Hone J 2010 *Nat. Nanotechnol.* **5** 722

[36] Yang W, Chen G, Shi Z, Liu C C, Zhang L, Xie G, Cheng M, Wang D, Yang R, Shi D, Watanabe K, Taniguchi T, Yao Y, Zhang Y and Zhang G 2013 *Nat. Mater.* **12** 792

[37] Lin Y C, Ghosh R K, Addou R, Lu N, Eichfeld S M, Zhu H, Li M Y, Peng X, Kim M J, Li L J, Wallace R M, Datta S and Robinson J A 2015 *Nat. Commun.* **6** 7311

[38] Zhang C, Chu C P, Ren X, Li M Y, Li L J, Jin C, Chou M Y and Shih C K 2017 *Sci. Adv.* **3** 1601459

[39] Liu L, Sun Y, Cui X, Qi K, He X, Bao Q, Ma W, Lu J, Fang H, Zhang P, Zheng L, Yu L, Singh D J, Xiong Q, Zhang L and Zheng W 2019 *Nat. Commun.* **10** 4472

[40] Liu J, Huang Q, Qian Y, Huang Z, Lai F, Lin L, Guo M, Zheng W and Qu Y 2016 *Cryst. Growth Des.* **16** 2052

[41] Zhuang A, Li J J, Wang Y C, Wen X, Lin Y, Xiang B, Wang X and Zeng J 2014 *Angew. Chem.* **53** 6425

[42] Fan X, Jiang Y, Zhuang X, Liu H, Xu T, Zheng W, Fan P, Li H, Wu X, Zhu X, Zhang Q, Zhou H, Hu W, Wang X, Sun L, Duan X and Pan A 2017 *ACS Nano* **11** 4892

[43] Zhang L, Liu K, Wong A B, Kim J, Hong X, Liu C, Cao T, Louie S G, Wang F and Yang P 2014 *Nano Lett.* **14** 6418

[44] Shearer M J, Samad L, Zhang Y, Zhao Y, Puretzky A, Eliceiri K W, Wright J C, Hamers R J and Jin S 2017 *J. Am. Chem. Soc.* **139** 3496

[45] Yan C, Gan L, Zhou X, Guo J, Huang W, Huang J, Jin B, Xiong J, Zhai T and Li Y 2017 *Adv. Funct. Mater.* **27** 1702918

[46] Xia J, Zhu D, Wang L, Huang B, Huang X and Meng X M 2015 *Adv. Funct. Mater.* **25** 4255

[47] Madoune Y, Yang D B, Ahmed Y, Al-Makeen M M and Huang H 2023 *Front. Chem.* **11** 1132567

[48] Ahn J, Ha S, Choi J, Yeom D and Yoo Y 2023 *Adv. Optical Mater.* **11** 2203116

[49] Ouyang D C, Zhang N, Li Y and Zhai T Y 2023 *Adv. Funct. Mater.* **33** 2208321

[50] Kim K, DaSilva A, Huang S, Fallahazad B, Larentis S, Taniguchi T, Watanabe K, LeRoy B J, MacDonald A H and Tutuc E 2017 *Proc. Natl. Acad. Sci. USA* **114** 3364

[51] Bistritzer R and MacDonald A H 2011 *Proc. Natl. Acad. Sci. USA* **108** 12233

[52] Wu F, Lovorn T, Tutuc E and MacDonald A H 2018 *Phys. Rev. Lett.* **121** 026402

[53] Wu F, Lovorn T and MacDonald A H 2017 *Phys. Rev. Lett.* **118** 147401

[54] Tarnopolsky G, Kruchkov A J and Vishwanath A 2019 *Phys. Rev. Lett.* **122** 106405

[55] Kang J, Li J, Li S S, Xia J B and Wang L W 2013 *Nano Lett.* **13** 5485

[56] Chen M, Guo G C and He L 2010 *J. Phys.: Condens. Matter* **22** 445501

[57] Li P, Liu X, Chen M, Lin P, Ren X, Lin L, Yang C and He L 2016 *Comp. Mater. Sci.* **112** 503

[58] Ma J and Wang L W 2015 *Nano Lett.* **15** 248

[59] Yu H, Liu G B, Tang J, Xu X and Yao W 2017 *Sci. Adv.* **3** e1701696

[60] Wu M, Qian X and Li J 2014 *Nano Lett.* **14** 5350

[61] Huder L, Artaud A, Le Quang T, de Laissardière G T, Jansen A G M, Lapertot G, Chapelier C and Renard V T 2018 *Phys. Rev. Lett.* **120** 156405

[62] Kresse G and Furthmüller J 1996 *Comput. Mater. Sci.* **6** 15

[63] Kresse G and Furthmüller J 1996 *Phys. Rev. B* **54** 11169

[64] Perdew J P, Burke K and Ernzerhof M 1996 *Phys. Rev. Lett.* **77** 3865

[65] Klimeš J, Bowler D R and Michaelides A 2010 *J Phys. Condens. Matter* **22** 022201

[66] Sun Y, Cheng H, Gao S, Sun Z, Liu Q, Liu Q, Lei F, Yao T, He J, Wei S and Xie Y 2012 *Angew. Chem. Inter. Edit.* **51** 8727

[67] Krukau A V, Vydrov O A, Izmaylov A F and Scuseria G E 2006 *J Chem. Phys.* **125** 224106